

Chemical sputtering of ATJ graphite induced by low-energy D_2^+ bombardment

L.I. Vergara *, F.W. Meyer, H.F. Krause

Physics Division, Oak Ridge National Laboratory, Oak Ridge, TN 37831-6372, USA

Received 15 June 2005; accepted 4 August 2005

Abstract

Results of chemical sputtering of ATJ graphite by impact of D_2^+ in the energy range 10–250 eV/D are presented. Our experimental approach is based on the use of a quadrupole mass spectrometer (QMS) which samples the partial pressures of selected mass species in the scattering chamber resulting from the incident ion beam. Based on in situ measurements of cracking patterns and QMS sensitivities using calibrated leaks, sputtering yields are presented for the production of methane and acetylene for sample temperatures of 300 K and 800 K. In the energy range 10–60 eV/D, CD_4 appears to be the dominant light stable hydrocarbon detected at room temperature. With increasing D_2^+ energy, its contribution is found to decrease, while the contribution of C_2D_2 is virtually unchanged. In contrast to what is observed for the sample at room temperature, at 800 K a dramatic increase in the CD_4 production is observed with increasing beam energy, which is also manifested in the production of C_2D_2 , although to a smaller degree.

© 2005 Elsevier B.V. All rights reserved.

PACS: 34.50.Dy; 52.20.Hv; 79.20.-m; 79.20.Rf

1. Introduction

Graphite, carbon-based materials and their surface etching processes have received a great deal of attention over the past three decades [1–14]. One application for these materials is in the development of fusion technology, where one of the critical problems is identification of materials for use in plasma-facing components. Because of their high thermal conductivity, excellent shock resistance, absence of melting, low activation, and low-atomic

number, carbon-based materials are very attractive candidates for such environments. Understanding of hydrogen uptake and erosion mechanisms of these materials over a broad temperature range when they are exposed to an intense flux of hydrogen atoms or ions is essential to assess the suitability of these materials for use in large thermonuclear fusion reactor devices.

Chemical and physical sputtering processes, which occur when thermal neutral atoms or ions of hydrogen collide with a carbonaceous solid, have a strong influence on the material lifetime. Chemical sputtering for hydrogen–carbon systems, which leads to the ejection of light hydrocarbon molecular species such as methane (CH_4) or acetylene (C_2H_2),

* Corresponding author. Tel.: +1 865 574 4781; fax: +1 865 574 1118.

E-mail address: vergarali@ornl.gov (L.I. Vergara).

is significant and strongly dependent on the surface temperature and the hydrogen impact energy. Previous hydrogen impact results obtained using pure pyrolytic or highly oriented pyrolytic graphites (maximum expected density 2.25 g/cc) have shown effective chemical erosion rates that strongly depend on the graphite orientation (i.e., basal vs. pyramidal morphologies) [1]. Results for these pure and dense graphites have also been observed to depend on surface preparation and thermal heat treatment (hysteresis effects) [1]; results may be affected as well by micro or nano surface structure, pitting, and/or grain boundary formation, which is difficult to quantify in laboratory experiments. Less information is available (see, for example, Refs. [11–14]) about chemical sputtering processes that occur when hydrogen interacts with the low-density ATJ form of graphite (~ 1.7 g/cc); this easily machined form is currently used in many commercial applications including the liner material of fusion reactor test devices.

In an attempt to close this gap in fundamental knowledge, we have initiated studies of chemical sputtering by low-energy hydrogen ions impinging on ATJ graphite. Our studies have as their focus the important energy regime below 200 eV/atom where the consequences of surface impact are the least well-known experimentally or theoretically for any form of graphite.

2. Experiment

All measurements were performed in a floating potential ultra-high vacuum chamber with base pressures in the 10^{-8} Pa range, into which decelerated ion beams from an ECR ion source can be directed, as previously described [15]. A sensitive quadrupole mass spectrometer was installed in the scattering chamber as shown in Fig. 1. The chamber housed, in addition, a time-of-flight analyzer previously used for binary-collision backscattering studies [16]. A grounded baffle between the front end of the QMS and the target sample prevented field penetration from the QMS ionizer section to the region immediately in front of the sample, which was traversed by the low-energy ion beams. This baffle also blocked the line-of-sight path from the sample into the analyzer, along which scattered projectiles at higher beam energies could enter and cause unwanted backgrounds in the measured mass spectra. An ATJ (UCAR Carbon Co.) graphite target (material presently employed on the DIII-D device

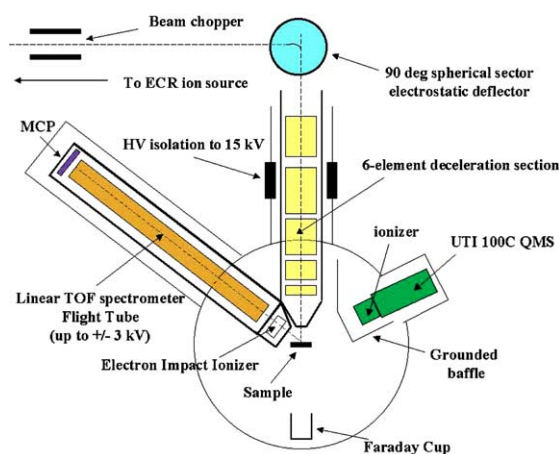


Fig. 1. Schematic diagram of the experimental apparatus.

at General Atomics) was used for all the measurements. The target was conditioned prior to mounting using the same procedure as was employed at DIII-D [17]. Target temperature variation was achieved by electron-beam-heating from the rear, and was monitored from the front using a calibrated infrared (IR) thermal monitor. Sample annealing at temperatures in excess of 1500 K was performed for about 45 s between measurements, in order to reinitialize the sample H/D inventory. The graphite sample was located 15 mm downstream of the electrostatic deceleration system. Mass selected beams of D_2^+ impacted the sample at normal incidence. The spatial profiles of the incident ion beams were approximately Gaussian with a width (FWHM) of 1–2 mm for the energy range 30–250 eV/D, and ~ 5 mm for 10 and 15 eV/D, as determined by a wire scanner that could be inserted in the plane of the target sample. From the beam currents intercepted by the sample and the beam profile measurements, typical beam fluxes of $2\text{--}8 \times 10^{19}$ D/(m² s) were inferred for the energy range of 30–250 eV/D. Fluxes in excess of 1×10^{18} D/(m² s) were obtained for energies as low as 10 eV/D. Typical vacuum during the measurements (i.e., with decelerated beam in the UHV chamber) was in the mid 10^{-7} Pa range.

The experimental approach used a sensitive quadrupole mass spectrometer which monitored the partial pressures of selected mass species in the 1–60 amu range present in the scattering chamber. A Macintosh-based data acquisition system was used to measure mass distributions at fixed intervals in time, or alternatively, to follow the intensities of selected mass peaks vs. beam exposure time. The evolution of peak intensities in the above mass

range was followed as a function of accumulated beam dose until saturation in their intensities occurred. It was crucial to the experimental approach that all contributions to the chamber pressure other than incident beam related ones be kept constant during the irradiation runs. This allowed the evolution of chemical sputtering products to be determined by taking differences between a pre-irradiation mass spectrum and mass spectra acquired during irradiation at progressively larger accumulated D target doses.

In the present article, measurements of mass spectra together with absolute calibrations of the QMS response for methane and acetylene were used to determine chemical sputtering yields of CD_4 and C_2D_2 for D_2^+ beams in the energy range 10–250 eV/D incident on samples at room temperature (RT) and at 800 K.

3. Interpretation of mass spectra

Fig. 2 shows a set of typical background-subtracted mass spectra for two sample temperatures, 300 K and 800 K, obtained with normally incident

D_2^+ beams at 60 and 250 eV/D. The spectra were obtained after attainment of steady state conditions, i.e., when the intensities of the various observed mass peaks no longer change with increasing D dose. In the figure, we see (not unexpectedly) that the dominant signal in each mass spectrum occurs at 4 amu (D_2) followed by smaller peaks at 2 and 3 amu (3–8 times smaller for different cases). Also evident, albeit at reduced intensities, are peaks at 18, 20 and 28 amu. The peaks at masses 20 and 28 are consistent with the production of stable molecular species such as CD_4 (methane) and C_2D_2 (acetylene). The peak at mass 18 is consistent with the formation of the CD_3 radical, or the formation of an isotopically mixed stable species such as CD_2H_2 .

In order to make our observations quantitative, we performed in situ measurements of hydrocarbon cracking patterns for CH_4 and C_2H_2 using UHV-compatible calibrated leaks. The measured cracking patterns for the latter hydrocarbons were found to be in good agreement with tabulated values for this instrument [18], which serves as justification for adopting the *tabulated* cracking patterns for heavier hydrocarbons like C_2D_4 , C_2D_6 , C_3D_6 , and C_3D_8 as

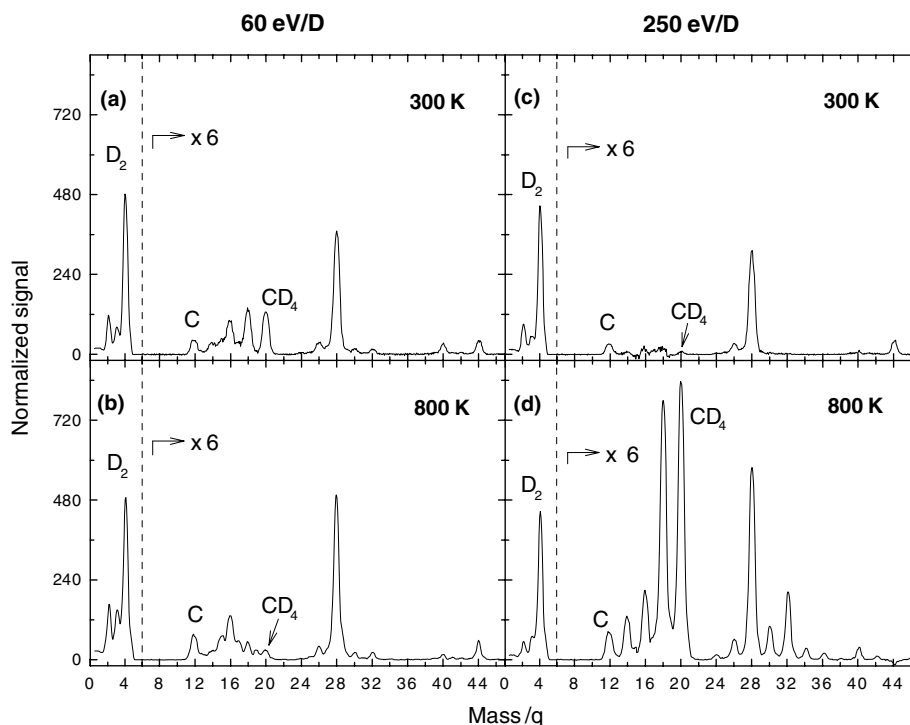


Fig. 2. Background-subtracted mass spectra obtained after saturation of all mass peak intensities for different beam energies and sample temperatures: (a) 60 eV/D and 300 K, (b) 60 eV/D and 800 K, (c) 250 eV/D and 300 K, and (d) 250 eV/D and 800 K. The normalized signal corresponds to mass peak amplitude divided by the incident beam current.

well. Inclusion of these heavier hydrocarbons in the analysis was required, because some of their cracking products can contribute to the peaks of interest.

Assuming that the hydrocarbon fragmentation is independent of H/D isotopic make-up, the CH_4 pattern observed with the calibrated methane leak confirmed that most of the intensity in the mass 18 peak observed in Fig. 2(a), (b) and (d) in fact arises from the cracking of CD_4 in the ionizer of the QMS. On the other hand, the contribution from C_2D_2 to the mass 28 peak intensity in all the spectra of Fig. 2 was found to be less than 30%. The majority of the peak intensity is due to species such as CO, CND, and/or N_2 , and to a lesser extent, to contributions from the cracking of heavier hydrocarbons.

A relatively straightforward method to determine the contributions to the measured chemical sputtering signal at a certain mass from the cracking of heavier hydrocarbons in the quadrupole analyzer involves the use of a matrix analysis of the sputtering signals such as that described by Davis et al. [4]. Such a matrix analysis is based on the selection of a single analysis mass for each included hydrocarbon species. In this paper, the selected analysis masses are (in amu): 20, 24, 30, 36, 46, and 34, for CD_4 , C_2D_2 , C_2D_4 , C_2D_6 , C_3D_6 , and C_3D_8 , respectively. At these masses, interferences due to non-hydrocarbon contaminants and cracking products from heavier hydrocarbons were found to be the smallest. Based on this selection, a 6×6 cracking pattern matrix, \mathbf{C} , was constructed, where each column represents the contribution of one of the selected hydrocarbons to the array of selected analysis masses, normalized to have unit intensity for its own analysis mass, as shown in Fig. 3. To determine

hydrocarbon	mass (amu)	CD_4	C_2D_2	C_2D_4	C_2D_6	C_3D_6	C_3D_8
20	1	0	0	0.02	0.02	0.004	
24	0	1	0.05	0.02	0.003	0.001	
30	0	0	1	1.375	0.46	0.42	
34	0	0	0.05	0.875	0.11	1	
36	0	0	0	1	0.01	0.025	
46	0	0	0	0	1	0.13	

Fig. 3. Cracking pattern matrix for deuterated hydrocarbons. Each column (hydrocarbon) is normalized to have unity intensity for the mass peak chosen as representative of each hydrocarbon (analysis mass).

the cracking contributions to the intensity of a particular analysis mass from other hydrocarbons, a deconvolution of the measured signal was then performed. This was achieved by forming the product $\mathbf{C}^{-1}\underline{\mathbf{s}}$, where \mathbf{C} is the above cracking matrix and $\underline{\mathbf{s}}$ is the array of measured peak heights (normalized to the incident ion flux, expressed in particles/s) at each analysis mass. In correcting the incident beam currents for secondary electron emission, γ values ranging from 0.05 to 0.2 were assumed for the different investigated energies, in order of increasing energy. Using this deconvolution procedure, it was found that the peak at mass 20 (i.e., the CD_4 analysis mass peak) is essentially free from interferences, and that the mass 24 peak (i.e., the C_2D_2 analysis mass peak) required less than 25% intensity correction due to the presence of cracking products of other hydrocarbon species.

To convert the deconvoluted intensities to yields, the normalized peak heights must be converted to production rates using the calibration of the QMS obtained via the standard leaks. The entire procedure (including both deconvolution and calibration) is expressed by the following equation:

$$\underline{\mathbf{y}} = \mathbf{R}(\mathbf{C}^{-1}\underline{\mathbf{s}}), \quad (1)$$

where $\underline{\mathbf{y}}$ is the end result, namely the apparent sputtering yield array for the selected hydrocarbons, and \mathbf{R} is the diagonal calibration matrix giving the conversion from QMS normalized peak height to production rate in particles/s. Since we only used two hydrocarbon leaks, the calibration matrix \mathbf{R} used had only two non-zero diagonal elements (which correspond to the calibration factors for CD_4 and C_2D_2). In the near future we plan to add calibrated leaks of the heavier hydrocarbons, which will allow us to determine chemical sputtering yields for those hydrocarbons as well.

In this manner the two (corrected) peak intensities at masses 20 and 24, together with the absolute QMS calibration, were used to determine the apparent sputtering yields for CD_4 and C_2D_2 . In order to obtain true sputtering yields, the effect of wall contributions to the selected mass peak intensities must be considered, as discussed in the following section.

4. Determination of wall contributions to the sputtering signals

When we bombard the graphite sample, a fraction of the incident deuterium ions is reflected from

the sample and impacts the walls of the vacuum chamber where it can form stable hydrocarbons from precursors adsorbed there that may be detected subsequently by the QMS. This is called the wall contribution to the measured signal, and it is necessary to quantify and subtract this portion in order to obtain the true graphite chemical sputtering yields.

In the present experiments, the wall contributions were evaluated and subtracted using the method applied by Mech et al. [7,19], which involves measuring the beam-off to beam-on transient at each mass of interest. Fig. 4 shows the intensity evolution for the Mass 20 signal (methane) when the sample is at room temperature, for two different beam energies: 60 eV/D (upper panel) and 10 eV/D (lower panel). When the beam is turned on, we observe a fast rise in the hydrocarbon signal (time constant of ~ 3 –5 s), followed by a slower increase having a time

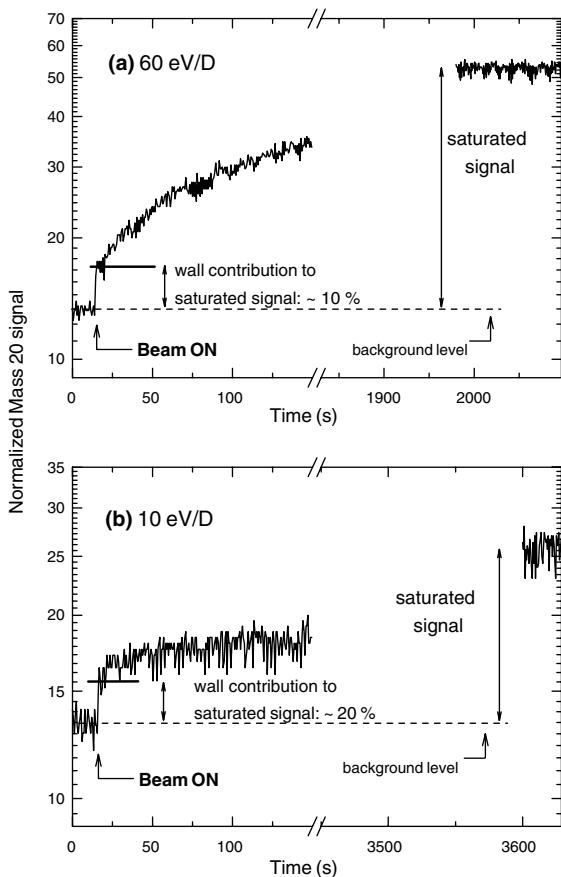


Fig. 4. Time evolution of the mass 20 peak intensity resulting from incidence of a D_2^+ beam at (a) 60 eV/D and (b) 10 eV/D for ATJ graphite at room temperature.

constant which depends on the beam energy. Immediately after the beam is turned on, the graphite sample is not hydrogenated, and therefore, the initial steep rise cannot be due to hydrocarbons originating from the sample. However, there are hydrocarbon precursors on the vacuum chamber walls due to previous measurements. This initial steep rise must therefore be attributed to hydrocarbon formation resulting from the interaction of the reflected deuterium with the walls. The subsequent slower increase is due to hydrocarbon formation on the sample as its deuterium inventory approaches the saturated state. From the analysis of the transients when the sample is at room temperature, we found that the initial steep increase represents at most 10% for energies higher than 60 eV/D, and at most 20% for energies as low as 10 eV/D. Doing the same study for the sample at high temperature (800 K), we obtain wall contributions that range from 30% at 15 eV/D to less than 5% at 250 eV/D. In order to determine the *true* chemical sputtering yields, the above wall contributions must be subtracted from the apparent yields discussed in Section 3.

Our values for the wall contribution are lower than the ones reported by Wright et al. [13], which range from 30% to 90% depending on the incident ion energy and sample temperature. The differences could be attributed to our limited use of deuterium beams in the chamber prior to the present investigations (less hydrocarbons precursors on the walls), to our lower background base pressure (4 – 5×10^{-8} Pa in our case vs. 1×10^{-6} Pa in the experiments of Wright et al.), and also, to our much lower chamber pressure during ion-beam loading (low 10^{-7} Pa in our case vs. 3 – 4×10^{-4} Pa in the experiments of Wright et al.).

5. Chemical sputtering yields

The methane and acetylene chemical sputtering yields due to D_2^+ impact on ATJ graphite are shown as a function of incident energy in Fig. 5(a) and (b), respectively. When the sample is at room temperature, the methane yield exhibits a broad plateau (~ 4 – 6×10^{-3} CD_4/D) at energies below ~ 60 eV/D and decreases as the energy is increased (4.0×10^{-4} CD_4/D at 250 eV/D). When the sample is at high temperature, the energy dependence of the methane production is opposite to the one observed at room temperature: CD_4 increases steeply when increasing the energy from 15 eV/D up to 250 eV/D.

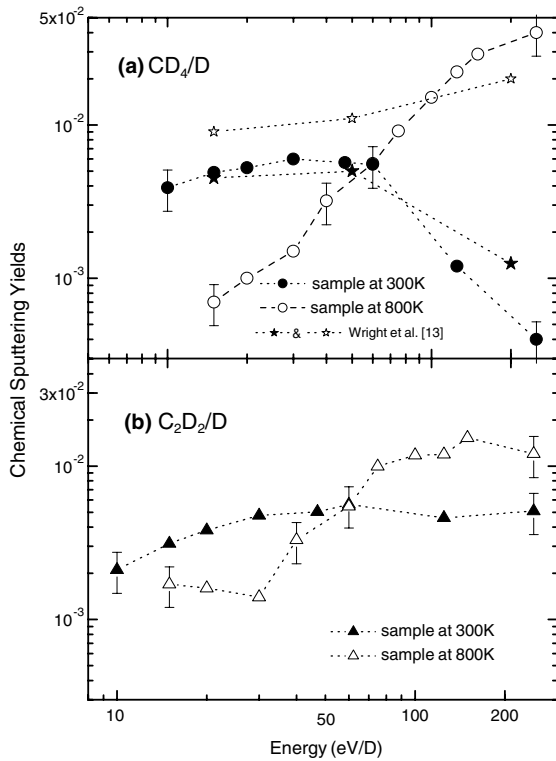


Fig. 5. Chemical sputtering yields of CD_4 and C_2D_2 for D^+ incident on ATJ graphite at room temperature and 800 K as function of the beam energy.

The acetylene yield for the room temperature case increases from $\sim 2.0 \times 10^{-3}$ to 5.0×10^{-3} when the energy is increased from 10 to 60 eV/D and then it remains almost constant for higher energies (within the experimental uncertainty of $\sim 30\%$). On the other hand, when the sample is at high temperature, the acetylene yield is essentially constant at energies below 30 eV/D, and then increases with energy from $\sim 1.4 \times 10^{-3}$ at 30 eV/D, up to $\sim 1.5 \times 10^{-2}$ at 100 eV/D, and then returns to a roughly flat energy dependence up to 250 eV/D.

Recently, Wright et al. presented CD_4 yields and temperature dependences for three beam energies within our covered energy range: 15, 50 and 200 eV/D [13]. These yields are also shown in Fig. 5(a). When the sample is at RT, the results show a very good agreement, except for the less pronounced decay presented by Wright et al.'s results when the beam energy is higher than 60 eV/D. In contrast, the methane yield energy dependence found when the ATJ graphite is at ~ 800 K is quite different when comparing the two sets of results, the difference approaching one order

of magnitude for the lowest energies. The reason for this discrepancy is presently not understood.

6. Discussion

For thermal energy H impact on a H saturated graphite surface, the chemical erosion is essentially determined by the competition between H and CH_3 release [20]. Both processes are thermally activated. As a result there is little observed chemical erosion at room temperature. Since the activation energy of H release is slightly higher than that for CH_3 release, the chemical erosion reaches a maximum value with increasing sample temperature and then decreases back to zero.

For energetic H impact, hydrogenation and methyl group formation has been shown to occur at the end of the impacting ions' range in the graphite bulk, i.e., after thermalization of the incident ions [21,22]. As a result, diffusion of methyl groups back to the surface plays an increasing role with increasing ion energy. Once the CH_3 reaction products reach the near surface region, their kinetic ejection by non-thermalized incident particles augments the erosion resulting from thermally activated CH_3 release [21–23].

In this context, some of the general features of the present data are now qualitatively discussed. At the lowest investigated energies, CD_4 production is very significant already for a room temperature sample, a clear demonstration of the importance of the above mentioned kinetic ejection mechanisms. Interestingly, at the lowest impact energies the observed CD_4 production at 800 K is almost an order of magnitude lower than that observed at room temperature, indicative of the increased competition of the thermally activated D release noted above. At room temperature, as the ion impact energy is increased above 60 eV/D, the CD_4 yield decreases significantly, suggesting decreased CD_3 survival during its diffusion back to the graphite surface. The methane yield for the 800 K sample temperature, on the other hand, increases strongly with increasing energy over the entire range investigated. One possibility for this dramatic increase could lie in the known strong increase of diffusion coefficients with temperature. A significantly reduced diffusion time of CD_3 back to the surface could increase their survival probability. In addition, the kinetic ejection itself may be slightly thermally activated, which would further enhance the production of free CD_4 .

In contrast, the energy dependences of the observed C_2D_2 yields are much weaker, as is the observed dependence on sample temperature. In the light of the above discussion, the flatter energy dependence suggests a reduced importance of diffusional processes for production of C_2D_2 , and thus implies production more closely confined to the graphite near surface region. A more detailed analysis of the temperature and energy dependences of the branching ratios for production of the different hydrocarbons, required to test this speculation, is beyond the scope of the present article.

7. Conclusions and outlook

Chemical sputtering yields of CD_4 and C_2D_2 , produced by the impact of D_2^+ normally incident on ATJ graphite, have been measured for beam energies in the range 10–250 eV/D, and at two different sample temperatures: 300 K and 800 K. For 300 K, the methane yield exhibits a broad plateau in the range 10–60 eV/D and then *decreases* at higher energies. In contrast, the acetylene yield remains constant to within a factor of two over the entire investigated energy range.

At a sample temperature of 800 K, the CD_4 yield at, e.g., 15 eV/D, is smaller than the corresponding room temperature yield by almost an order of magnitude, but *increases* steadily with increasing beam energy, exceeding the room temperature yield at 250 eV/D by almost two orders of magnitude.

Since ATJ graphite has a poorly ordered bulk and surface microstructure, at the lowest impact energies penetration distances may be significantly different for incident molecular ions compared to atomic ion impact. To test this hypothesis, sample temperature dependence measurements are planned in the near future with D^+ as well as D_3^+ ions incident on ATJ graphite at energies down to 10 eV/D. Complementary measurements with HOPG samples using very low-energy D^+ , D_2^+ , and D_3^+ beams will be carried out as well.

Acknowledgements

We are indebted to S.H. Overbury for making available the QMS and sample holder used in the

present measurements. This research was sponsored by the Office of Fusion Energy Sciences and the Office of Basic Energy Sciences of the US Department of Energy under Contract No. DE-AC05-00OR22725 with UT-Battelle, LLC. LIV was appointed through the ORNL Postdoctoral Research Associates Program administered jointly by Oak Ridge Institute of Science and Education and Oak Ridge National Laboratory.

References

- [1] M. Balooch, D.R. Olander, J. Chem. Phys. 63 (1975) 4772.
- [2] R. Yamada, J. Nucl. Mater. 145–147 (1987) 359.
- [3] E. Vietzke, K. Flashkamp, V. Philipps, G. Esser, P. Wienhold, J. Winter, J. Nucl. Mater. 145–147 (1987) 443.
- [4] J.W. Davis, A.A. Haasz, P.C. Stangeby, J. Nucl. Mater. 155–157 (1988) 234.
- [5] S. Chiu, A.A. Haasz, J. Nucl. Mater. 208 (1994) 282.
- [6] B.V. Mech, A.A. Haasz, J.W. Davis, J. Nucl. Mater. 241–243 (1997) 1147.
- [7] B.V. Mech, A.A. Haasz, J.W. Davis, J. Nucl. Mater. 255 (1998) 153.
- [8] M. Balden, J. Roth, J. Nucl. Mater. 280 (2000) 39.
- [9] E. Vietzke, J. Nucl. Mater. 290–293 (2001) 158.
- [10] T. Zecho, B.D. Brandner, J. Biener, J. Küppers, J. Phys. Chem. B 105 (2001) 6194.
- [11] J.W. Davis, P.B. Wright, R.G. Macaulay-Newcombe, A.A. Haasz, C.G. Hamilton, J. Nucl. Mater. 290–293 (2001) 66.
- [12] P.B. Wright, J.W. Davis, R.G. Macaulay-Newcombe, C.G. Hamilton, A.A. Haasz, J. Nucl. Mater. 313–316 (2003) 158.
- [13] G.M. Wright, A.A. Haasz, J.W. Davis, R.G. Macaulay-Newcombe, J. Nucl. Mater. 337 (2005) 74.
- [14] F.W. Meyer, H.F. Krause, L.I. Vergara, J. Nucl. Mater. 337 (2005) 922.
- [15] V.A. Morozov, F.W. Meyer, Rev. Sci. Instrum. 70 (1999) 4515.
- [16] V.A. Morozov, F.W. Meyer, Phys. Rev. Lett. 86 (2001) 736.
- [17] Todd Evans, private communication, GA QA Spec # 4-2106.15TS.
- [18] UTI 100C operating manual.
- [19] Brian Vernon Mech, PhD thesis, Department of Aerospace Studies, U. Toronto, June 1997, p. 52, unpublished.
- [20] J. Küppers, Surf. Sci. Rep. 22 (1995) 249.
- [21] J. Roth, C. Garcia-Rosales, Nucl. Fusion 36 (1996) 1647.
- [22] B.V. Mech, A.A. Haasz, J.W. Davis, J. Appl. Phys. 84 (1998) 1655.
- [23] C. Hopf, A. von Keudell, W. Jacob, Nucl. Fusion 42 (2002) L27.